Pharmacologically inducing regenerative cardiac cells by small molecule drugs

Wei Zhou[1,2,†], Kezhang He[b,†], Chiyin Wang[3], Pengqi Wang[2], Dan Wang[2], Bowen Wang[1,2], Han Geng[2], Hong Lian[3], Tianhua Ma[2]*, Yu Nie[3]*, Sheng Ding[1,2,4]*

Affiliations

[1]Tsinghua-Peking Joint Center for Life Sciences, Tsinghua University, Beijing 100084, China

[2]School of Pharmaceutical Sciences, Tsinghua University, Beijing 100084, China

[3]State Key Laboratory of Cardiovascular Disease, Fuwai Hospital, National Center for Cardiovascular Disease, Chinese Academy of Medical Sciences and Peking Union Medical College, Beijing, 100037, China

[†]W.Z. and K.Z.H. contributed equally to this work.

[4]Lead contact

*Corresponding author. Email: matianhua@tsinghua.edu.cn (T.M.), nieyu@fuwaihospital.org (Y.N.), shengding@tsinghua.edu.cn (S.D.)

Summary

In contrast to lower organisms, adult mammals cannot regenerate damaged hearts through de-differentiation of cardiomyocytes (CMs) into cells with regenerative capacity. Development of an enabling condition to induce such naturally unavailable cells with potential to proliferate and differentiate into CMs, i.e., regenerative cardiac cells (RCCs), in mammals will provide new insights and tools for heart regeneration. Here, a two-compound combination (2C), CHIR99021 and A-485, was identified to robustly induce RCCs from human embryonic stem cell (hESC) derived TNNT2^{+} CMs *in vitro*, which was confirmed by lineage tracing experiments. Functional analyses revealed that RCCs expressed a spectrum of genes essential for cardiogenesis and exhibited potential to become functional CMs, endothelial cells (ECs) and smooth muscle cells (SMCs). Consistent with the results in human cells, 2C-induced generation of RCCs were also observed in neonatal rats CMs *in vitro* and *in vivo*. Remarkably, administration of 2C can induce RCCs in adult mouse hearts and significantly improve survival and heart function in the mice undergoing myocardial infarction. Mechanistically, CHIR99021 is indispensable for transcriptional and epigenetic activation of genes essential for RCC, whereas A-485 mainly function to epigenetically down-regulate H3K27Ac and particularly H3K9Ac in CMs. Their combination specifically enhances both H3K27Ac and H3K9Ac on RCC genes, facilitating the establishment of RCC state dedifferentiated from CMs. Therefore, our findings demonstrated the feasibility and revealed the mechanisms of pharmacological induction of RCCs from endogenous CMs, which could offer a promising regenerative strategy to repair injured hearts.

Main Text

Lower organisms, such as zebrafish, possesses a robust cardiac regeneration capacity through CM dedifferentiation characterized by reactivation of embryonic cardiogenic genes and disassembly of their sarcomeric structures (Kikuchi & Poss, 2010; Lepilina *et al*, 2006). In contrast, limited cardiac regeneration was only permitted from postnatal day 1 to day 6 (PN1 to PN6) in mice with sarcomeric disassembly and proliferation of CMs in the resected section of heart (Porrello *et al*, 2011), which is no longer observed beyond this narrow time window. Therefore, discovery of small molecule drugs enabling induction of regenerative capacity in mammalian adult endogenous CMs by recapitulating the regenerative cellular state presented in zebrafish will shed mechanistic lights on the understanding of roadblocks preventing CMs from dedifferentiation in mammalian hearts, and facilitate development of regenerative medicine to treat various heart diseases caused by CM loss.

During mammalian heart development, cardiomyocytes (CMs) mainly originate from first heart field (FHF) and second heart field (SHF) (Srivastava, 2006). In particular, SHF cells marked by the pioneer transcription factor ISL1 can proliferate and differentiate into three major cardiovascular cell types, CMs, SMCs and ECs during embryonic heart development (Bu *et al*, 2009; Moretti *et al*, 2006). Consistently, a small number of ISL1$^+$ cells residing in the neonatal mouse heart between postnatal Day 1 and Day 5 were reported to expand and differentiate into CMs under appropriate *in vitro* conditions (Laugwitz, 2005). Since ISL1 transcriptionally governs the expression of a cohort of cardiac genes, e.g., *NKX2-5* (Ma *et al*, 2008), *FGF10* (Watanabe *et al*, 2012), essential for embryonic cardiogenesis, it is reasonable to hypothesize that induced expression of ISL1 in CM may be a determinative step in the induction of regenerative cardiac cells (RCCs).

Toward induction of regeneration capacity in CMs, we conducted a screening for small molecules that can induce the expression of ISL1 in CMs. Our combinatorial screening identified a novel combination of CHIR99021 and A-485/2C that could unprecedentedly and efficiently induce dedifferentiation of human CMs into RCCs. These RCCs exhibited disassembled sarcomeric structures, high expression of embryonic cardiogenic genes, and increased number of CMs through re-differentiation *in vitro*. Further studies showed that 2C could robustly generate RCCs in hearts of adult mice and improve cardiac function in the mice with myocardial infarction. Our proof-of-concept discovery demonstrated that a simple combination of small molecule drugs can grant regenerative capacity to the heart by reprogramming CMs into RCCs.

2C treatment efficiently induces dedifferentiation of hESC-derived CMs

To obtain an adequate number of CMs for small molecule screening, we differentiated hESCs into CMs (*SI Appendix,* Fig. S1*A* and Movie S1) following a well-established step-wise protocol (Lian *et al*, 2013). Consistent with previous reports, nearly homogenous contracting CMs were observed on day 10 of differentiation. After purification with glucose-depleted medium containing abundant lactate (*SI Appendix,* Fig. S1*B*), highly pure TNNT2$^+$ CMs were obtained, and then subsequently dissociated and seeded into 96-well plates. When CMs resumed contraction, they were treated with individual small molecules from a

68 collection of over 4,000 compounds for 3 days (*SI Appendix,* Fig. S1*C* and Table S1), and then fixed and
69 immunostained with ISL1. Using a high-content imaging (HCI) and analysis system, five compounds were
70 initially identified to potentially induce regenerative capacity in CMs, indicated by induced sarcomere
71 disassembly and ISL1 expression (*SI Appendix,* Fig. S1*D*). After further comparing the effects from various
72 combinations, the unique combination of CHIR99021 and A-485 (2C) was found to most efficiently induce
73 ISL1 expression with healthy cell state (*SI Appendix,* Fig. S1*E*).

74 When CMs with well-organized sarcomeres were treated with 2C *in vitro*, cells started to exhibit
75 dedifferentiation-associated phenotype, such as reduction of cell size after 24 hours and growing as clusters
76 after 48 hours and forming colonies after 60 hours (Fig. 1*A* and *SI Appendix,* Fig. S2 *A-C*). During this time,
77 the expression of TNNT2 and MYL2 were gradually downregulated while ISL1 expression and the
78 percentage of ISL1$^+$ cells were gradually increased (*SI Appendix,* Fig. S2 *D-G*). Compared to untreated
79 CMs, significant sarcomere disassembly and reduction of cytoplasmic/nuclear area were observed in cells
80 treated with 2C for 60 hours (Fig. 1 B-D). In parallel, the number and percentage of TNNT2$^+$ cells remained
81 constant while ISL1$^+$ cells increased remarkably (Fig. 1 *E-G*), accompanied by a ~3-fold increase ISL1
82 expression at both mRNA and protein levels (Fig. 1 *H-J*). Of note, other typical genes involved in early
83 embryonic cardiogenesis, including MESP1, LEF1 (Klaus *et al*, 2007), FUT4 (Wang *et al*, 2019), and NR2F2
84 (Churko *et al*, 2018) were also induced by 2C to express at high levels (Fig. 1*J* and *SI Appendix,* Fig. S2*H*).
85 In addition, treatment with 2C resulted in significantly decreased expression of CM-specific genes, such as
86 TNNT2, MYL2, MYL7, and MEF2C, while the pan-cardiac transcription factors, GATA4, TBX5, and NKX2-
87 5, showed no obvious expression changes (Fig. 1*J* and *SI Appendix,* Fig. S2*H*). Furthermore, when we
88 generated mature CMs from hESCs by treating differentiating cells with ZLN005 following a previously
89 reported method (Liu *et al*, 2020), 2C could induce ISL1 expression in these mature CMs (*SI Appendix,* Fig.
90 S2*I*). These results suggested that CMs might be converted by 2C into a state with regenerative capacity.

91 **2C induced cells possess regenerative capacity**

92 To confirm the regenerative capacity of 2C-induced cardiac cells, we investigated cell proliferation using a
93 BrdU incorporation assay. Immunostaining clearly showed the co-localization of ISL1 and BrdU labeling in
94 cells (Fig. 2*A*), and subsequent statistical analysis revealed a significant decrease in the nuclear area and
95 increase in the cell percentage of ISL1$^+$/BrdU$^+$ positive cells following 2C treatment (Fig. 2 *B* and *C*). We
96 next examined the potential for re-differentiation of 2C-induced cardiac cells into CMs. As expected, upon
97 withdrawal of 2C and subsequent culture in CM media for 3 days (60h+3d), we observed the emergence
98 of spontaneously contracting cells exhibiting CM-specific morphology with typical size of
99 cytoplasmic/nuclear area (Fig. 2 *D-F* and Movie S2), downregulated expression of early embryonic
100 cardiogenesis genes and upregulated expression of CM-specific genes, and the expression of pan-cardiac
101 genes didn't show any noticeable changes throughout this process (*SI Appendix,* Fig. S3*A*). Remarkably,
102 there was a 1.4-fold increase in the number of re-differentiated CMs with clear TNNT2 staining relative to
103 the initial CMs before 2C treatment (Fig. 2 *G* and *H*), demonstrating a regenerative potential in 2C-induced
104 cardiac cells. In addition to CMs, 2C-induced cardiac cells were capable of differentiation towards SMA$^+$

105 SMCs or CD31$^+$/VE-Cadherin$^+$ ECs in the presence of PDGF-BB and TGF-β1 or VEGF, bFGF and BMP4,
106 respectively (Fig. 2*I* and *SI Appendix,* Fig. S3 *B-D*). In contrast, the expression of those genes was not
107 detectable in DMSO-treated cells. Collectively, our findings indicate that treatment with 2C facilitates the
108 conversion of CMs into cardiac cells with regenerative capability, including proliferative potential and ability
109 to differentiate into the three major cardiovascular cell types, which were therefore named as regenerative
110 cardiac cells (RCCs).

111 **Lineage tracing demonstrated that 2C induced RCCs dedifferentiated from TNNT2$^+$ CMs**

112 Although TNNT2$^+$ CMs purified by lactate-based culture medium were almost homogeneous populations,
113 we noticed that these were still a low percentage (<4%) of purified cells still expressed ISL1 (*SI Appendix,*
114 Fig. S1*B*). Therefore, we performed lineage-tracing experiments to further confirm that the 2C-induced
115 RCCs were actually dedifferentiated from TNNT2$^+$ CMs rather than proliferation of those residual ISL1$^+$
116 cells. Upon directed cardiac differentiation of an ISL1$^{mCherry/+}$ H9 hESC (K9) line established through
117 CRISPR-based knock-in (*SI Appendix,* Fig. S4 *A-D*), mCherry expression faithfully reflected endogenous
118 ISL1 expression (Fig. 3 *A-C*). After purification of K9-derived CMs, mCherry-negative cells were selected
119 by FACS (Fig. 3 *D* and *E*), all of which were confirmed to be TNNT2$^+$ CMs (*SI Appendix,* Fig. S4*E*). Those
120 mCherry-negative CMs were then treated with 2C for 60 hours. The expression of TNNT2 and MYL2 were
121 dramatically down-regulated, whereas the expression of ISL1 and mCherry was significantly up-regulated
122 (Fig. 3 *F* and *K*). We found the induced mCherry$^+$/ISL1$^+$ RCCs exhibited significant morphological changes
123 accompanied by a dramatic decrease in TNNT2 expression (Fig. 3*F*). In contrast, the mCherry-negative
124 CMs remained high expression of TNNT2 with the typical sarcomere structure (Fig. 3*F*). FACS analysis
125 further confirmed that 2C was capable of K9-derived mCherry-negative CMs into mCherry$^+$/ISL1$^+$ cells (Fig.
126 3 *G* and *H*). Consistently, similar results were observed using HUES7 hESC line with ISL1-mCherry knock-
127 in reporter (K7) (Fig. 3 *I*, *J*, *L*, and *SI Appendix,* Fig. S5).

128 Furthermore, we used a lineage-tracing system to unequivocally examine the conversion of CMs to
129 ISL1-expressing RCCs by 2C treatment. In this assay, CMs were transfected with plasmids encoding
130 CreERT2 under the control of TNNT2 promoter and an EGFP reporter following flox-stop-flox cassette (*SI*
131 *Appendix,* Fig. S6*A*). After optimizing virus titer and infection time (*SI Appendix,* Fig. S6 *B-D*), ~0.6 of K9-
132 derived mCherry-negative CMs were permanently labeled with EGFP following 6 days of treatment with
133 tamoxifen (Fig. 3 *M* and *N*). Then, those EGFP-labeled mCherry-negative CMs were sorted by flow
134 cytometry and subsequently treated with 2C for 60 hours. As expected, the expression of ISL1 was
135 observed in these EGFP$^+$ CMs (Fig. 3*O*). Collectively, these results robustly demonstrated that RCCs with
136 ISL1 expression were truly generated by 2C treatment from TNNT2$^+$ CMs.

137 **2C-induced dedifferentiation of CMs provided a protective effect on cardiac infarction**

138 In order to examine 2C's reprogramming effect on CMs *in vivo*, we first tested 2C on primary neonatal rat
139 CMs (Sakurai *et al*, 2014), on which 2C was found to consistently induce RCCs generation with
140 corresponding ISL1 induction and morphological changes (*SI Appendix,* Fig. S7*A*). Then, we sought to

141 examine whether 2C was capable of reprograming endogenous CMs to RCCs *in vivo*. For this purpose,
142 neonatal SD rats were intraperitoneally administrated with 20 mg/kg of CHIR99021 and 10 mg/kg of A-485
143 daily for 5 days (*SI Appendix,* Fig. S7*B*). Compared to the vehicle/DMSO controls (NC), ISL1 was robustly
144 induced in the cells from hearts of rats treated with 2C without apparent effects on body weight (*SI*
145 *Appendix,* Fig. S7 *C* and *D*). These induced ISL1-expressing cells were widely distributed within the region
146 600 μm to 3000 μm down from the base of the hearts, including aorta (Ao), left/right atria, and both ventricles
147 (*SI Appendix,* Fig. S7*E*). Notably, all of these $ISL1^+$ expressed TNNT2 as well, strongly indicating 2C-
148 induced RCCs were actually originated from CMs *in vivo*. More importantly, neither administration of 20
149 mg/kg CHIR99021 nor 10 mg/kg A-485 alone observed $ISL1^+$ cells in ventricles, powerfully illustrating the
150 combined effect of 2C on the induction of RCCs (*SI Appendix,* Fig. S8).

151 Similarly, RCCs were also efficiently induced in the Ao root and RA regions of the heart dissected from
152 adult 129SvJ mice administrated with 2C (20 mg/kg of CHIR99021 and 10 mg/kg of A-485) for 5 consecutive
153 days as well (Fig. 4*A*). Intriguingly, we sought to explore whether 2C-inced RCCs could rescue cardiac
154 function in mice subjected to myocardial infarction (MI). In a prophylactic setting, mice were pre-treated
155 with either 2C or vehicle/DMSO for 5 days (Fig. 4*B*) and then inducing MI by ligation of left anterior
156 descending (LAD) artery. When measuring cardiac function with magnetic resonance imaging (MRI) on
157 days 1, 8, 25 and 35 post-MI, we found pretreatment with 2C was able to significantly improve both cardiac
158 function and survival rate in the mice, without affecting their body weight (Fig. 4 *C*-*E*). Next, when we treated
159 mice with 2C or vehicle/DMSO post-MI in a therapeutic setting (Fig. 4*F*), remarkably mice with 2C treatment
160 displayed a recovered cardiac function as assessed by both left ventricular ejection fraction (LVEF) and
161 echocardiography (Fig. 4 *G* and *H*). Consistently, cardiac fibrosis was largely ameliorated in 2C-treated
162 mice that displayed significantly smaller scar size in the hearts compared to control mice (Fig. 4*I*). Those *in*
163 *vivo* studies collectively indicate that 2C or further improved small molecule drugs with similar mechanisms
164 may have therapeutic utility to repair or regenerate hearts after cardiac injury. Altogether, these *in vivo*
165 studies indicate that 2C-induced RCCs possess the same regenerative capacities comparable to those
166 generated *in vitro,* which will shed light on development of small molecule drugs with therapeutic utility to
167 repair or regenerate hearts after cardiac injury.

168 **Both CHIR99021 and A-485 are required to induce dedifferentiation of CMs to RCCs**

169 To gain insights into mechanisms involved in 2C-induced dedifferentiation of CMs to RCCs, we performed
170 bulk RNA-seq analysis of K9-derived ISL1/mCherry-negative CMs treated with DMSO (NC) or 2C for 60
171 hours (Fig. 5*A*). Analysis of differentially expressed genes (DEGs) revealed a remarkable change in the
172 transcriptome upon 2C treatment (Fig. 5*B*). In detail, 2C treatment led to increased expression of a large
173 set of genes known to be associated with embryonic cardiogenic genes (e.g., MSX1, BMP4, TCF4, and
174 LEF1) and suppression of a significant list of genes associated with CMs (Fig. 5*C*). Consistently, gene
175 ontology (GO) analysis further revealed that down-regulated genes were mainly involved in cardiac
176 maturation and muscle contraction (Fig. 5*D*), while up-regulated genes were enriched in cell junction and
177 catenin complex (Fig. 5 *E* and *F*). Those embryonic cardiogenic genes and other genes significantly up-

178 regulated (e.g., MSX2, NKD1, PDGFC, CTNNA2) after 2C treatment were confirmed by qPCR in K9-
179 derived mCherry-negative CMs (Fig. 5*G*).

180 To investigated the individual effects of CHIR99021 and A-485 on induction of RCCs, we compared
181 H9 hESC-derived CMs treated with CHIR99021 and A-485 individually or in combination. When measuring
182 cytoplasmic/nuclear area, we found CHIR99021 significantly reduced both cytoplasmic and nuclear area,
183 a distinguishable morphological feature of RCCs, in comparison to A-485 that only reduced cytoplasmic
184 area (*SI Appendix,* Fig. S9 *A*-*C*). Consistently, disassembly of sarcomere structures was more frequently
185 observed in CMs treated with CHIR99021 than in CMs treated with A-485 (*SI Appendix,* Fig. S9*E*). Although
186 reduced expression of TNNT2 and MYL2 as well as increased expression of ISL1 can be induced
187 individually by CHIR99021 and A-458 (*SI Appendix,* Fig. S9 *D* and *E*), CHIR99021 was able to uniquely
188 promote the expression of a cohort of genes involved in embryonic cardiogenesis, including BMP4, NKD1,
189 MSX2, PDGFC, LEF1 and TCF4 (*SI Appendix,* Fig. S9*D*). Upon withdrawal of CHIR99021, A-485 or 2C,
190 the cell percentage of $ISL1^+$ cell was similarly and significantly reduced (*SI Appendix,* Fig. S9*F*). Of note, a
191 drastic increase in the number of $TNNT2^+$ CMs was only observed in redifferentiation of 2C-treated cells,
192 as confirmed by statistical analysis (*SI Appendix,* Fig. S9*G*). These findings suggested that CHIR99021
193 played a leading role in 2C-induced de-differentiation of CMs to RCCs, A-485 is also indispensable.

194 **Reprogramming of CMs to RCCs by 2C went through an intermediate cell state**

195 Next, we performed scRNA-seq of K9-derived mCherry-negative CMs treated with DMSO (NC) or 2C for
196 60 hours. Utilizing UMAP analysis, we observed the proportion of cells within three (cluster 0, 2, 3) out of 7
197 identified clusters increased after 2C treatment (Fig. 6 *A* and *B*). Among these three clusters, cells in cluster
198 2 highly expressed RCC characteristic genes, including those essential for embryonic cardiogenesis (*e.g.,*
199 ISL1, BMP4 and FGF20 (a key gene involved in expansion of early embryonic progenitor cells (Cohen *et*
200 *al*, 2007)), and cell proliferation marker gene MKI67 (Fig. 6 *C* and *D*). By contrast, cells in cluster 0, 3, 4,
201 and 5 expressed CMs specific markers (*e.g.,* MYH6 and MYL2) at high levels (Fig. 6 *C* and *D*), indicating
202 they were CMs. Meanwhile, cells in cluster 1 and 6 were considered as intermediate cells (ICs) during 2C-
203 induced reprogramming of CMs to RCCs, because of expression of ACTA2, a marker gene reported to
204 express in CM dedifferentiation, and genes associated with CM development, including COL1A1, COL1A2,
205 and COL3A1 (Cui *et al*, 2020; Mononen *et al*, 2020) (Fig. 6 *C* and *D*).

206 When further examining cluster 2 with 435 cells from DMSO-treated cells and 410 cells from 2C-
207 treated cells by second-level clustering analysis, we identified subcluster 0 (408, or 48.3% out of 845 cells)
208 in cluster 2 which was exclusively observed in 2C-treated cells (Fig. 6 *E and F*). Furthermore, cells in
209 subcluster 0 expressed a series of RCC-related genes essential for embryonic cardiogenesis, including
210 MSX1, LEF1, BMP4, MSX2, and HAND1 (Fig. 6*G*), as well as a series of genes co-expressed with ISL1 in
211 SHF progenitors *in vivo*, such as NR2F2, TBX5, ALCAM (Ghazizadeh *et al*, 2018), and CXCR4 (Andersen
212 *et al*, 2018) (Fig. 6*G*), strongly indicating cells in subcluster 0 represent RCCs induced by 2C treatment.
213 Thus, a unique gene set that included LIX1, NKD1, PDGFC, ARL4A, AXIN2, FZD7, ISL1, MSX1, MSX2,
214 BMP4, LEF1, and HAND1 was found to determine RCC state during the reprogramming of CMs by 2C, and

215 hence designated as RCC genes. In addition, the pseudo-time analysis that clearly revealed 2C-induced
216 reprogramming of CMs (highly expressing TNNT2) went through ICs (highly expressing COL1A1), and
217 ultimately towards RCCs (highly expressing ISL1 and FGF20) (Fig. 6 *H-I*).

218 **RCC and CM genes were epigenetically regulated by 2C during reprogramming of CMs into RCCs**

219 As a p300 acetyltransferase inhibitor, A-485 was previously reported to specifically inhibit acetylation of H3
220 at lysine 27 (H3K27Ac) but not at lysine 9 (H3K9Ac) in the PC3 cells (Lasko *et al*, 2017). Consistently, the
221 percentage of H3K27Ac$^+$ cells but not that of H3K9Ac$^+$ cells were specifically and significantly reduced in
222 CMs were treated with A-485 alone (*SI Appendix,* Fig. S10). In contrast, neither CHIR99021 nor 2C
223 treatment resulted in noticeable alterations in the percentage of H3K27Ac$^+$ and H3K9Ac$^+$ cells (*SI Appendix,*
224 Fig. S10). Intriguingly, further analyses revealed a remarkable reduction in the levels of H3K27Ac and
225 H3K9Ac in TNNT2$^+$ cells following A-485 treatment (*SI Appendix,* Fig. S10 *F* and *L*), suggesting that A-485
226 simultaneously inhibit both H3K27Ac and H3K9Ac on CM-specific genes during the dedifferentiation of CMs.

227 To gain more insights on the mechanism underlying 2C-induced silencing of CM genes and activation
228 of RCC genes during reprogramming of CMs to RCCs, we performed chromatin immunoprecipitation-
229 sequencing (ChIP-seq) analyses of H3K27Ac and H3K9Ac in DMSO, A-485, CHIR99021 and 2C-treated
230 H9 hESC-derived CMs (Fig. 7*A*). We identified active promoters as proximal regions (±4 kb from the
231 transcription start sites, or TSS) exhibiting H3K4me3 enrichment in the cells treated with DMSO or 2C (Fig.
232 7 *B*, and *C*). Treatment with 2C led to a striking increase in H3K9Ac and H3K27Ac enrichment around TSS
233 regions on a whole-genome-wide scale (Fig. 7 *B* and *C*). Consistently, 2C treatment induced a significantly
234 enhanced enrichment of H3K9Ac in 4,485 genes and H3K27Ac enrichment in 2,560 genes, whereas a
235 decreased of H3K9Ac and H3K27Ac enrichment was detected in 346 and 1,834 genes respectively (*SI*
236 *Appendix,* Fig. S11 *A-F*). Of note, a significant part of genes decreased H3K9Ac (268, or 58.1% out of 461)
237 and H3K27Ac (777, or 68.6% out of 1132) enrichment in A485-treated cells were also observed among
238 genes that H3K9Ac (268, or 77.5% out of 346) and H3K27Ac (777, or 42.4% out of 1834) enrichment
239 following 2C treatment. Further GO analysis revealed that those genes decreased H3K9Ac and H3K27Ac
240 enrichment in their promoters commonly seen in repose to A-485 or 2C treatment, preferentially exhibited
241 cardiac specific functions, such as cardiac muscle contraction, sarcomere organization, and heart
242 contraction (*SI Appendix,* Fig. S11 *G-L*). Compared to individual treatment with A-485 or CHIR99021, 2C
243 treatment resulted in an increased H3K9Ac and H3K27Ac enrichment in the genes associated with cell
244 cycle and cell division (*SI Appendix,* Fig. S11 *K* and *L*), strongly supporting the combined effects of 2C on
245 RCC cell state establishment.

246 Next, we specifically examined H3K9Ac and H3K27Ac peaks in the promoters of critical CM genes
247 and RCC genes in the cells treated with or without A-485, CHIR99021 or 2C. We observed that both A-485
248 and CHIR99021 effectively reduced the peaks of H3K9Ac and H3K27Ac in the promoters of CM genes,
249 including TNNT2, TNNI1, MYL7, MYH6, and MYH7. These reductions were further intensified with 2C
250 treatment (Fig. 7*D and SI Appendix,* Fig. S12*A*). Interestingly, increased peaks of H3K9Ac and H3K27Ac
251 in promoters of the RCC genes, such as LEF1, AXIN2, BMP4, LIX1, MSX1, MSX2, and NKD1, was only

252 observed in condition with CHIR99021 available (Fig. 7*D and SI Appendix,* Fig. S12*B*). Other RCC genes,
253 including ISL1, ARL4A, FZD7, HAND1, and PDGFC, exhibited a significantly elevated peaks of H3K9Ac
254 and H3K27Ac by treatment with 2C and much higher than those treated with CHIR99021 alone (Fig. 7*D*
255 *and SI Appendix,* Fig. S12*C*). Therefore, while CHIR99021 was able to activate the expression of RCC
256 genes and simultaneously repressed CM genes partially through changing H3K27Ac and H3K9Ac during
257 2C-induced CM dedifferentiation to RCC, A-485 can inhibit CM genes directly through reducing of H3K27Ac
258 and H3K9Ac modifications in the promoters of CM-specific genes, thereby assisting CHIR99021 to
259 establish RCC state.

260 In addition, we observed that different small molecules had varied impacts on distribution of H3K9Ac
261 and H3K27Ac enrichment during 2C-induced dedifferentiation of CM into RCC. As indicated by Veen
262 diagram, distributions of H3K9Ac and H3K27Ac enrichment significantly diverged among cells treated with
263 DMSO, A-485, CHIR99021, and 2C (Fig. 7 *E* and *F*). For genes with H3K9Ac enrichment, 2716 (or 46.1%)
264 out of 5891 annotated genes were only enriched in the cells treated with 2C, while only 527 (or 4.9%) out
265 of 10785 annotated genes with H3K27Ac enrichment was exclusively observed (Fig. 7 *E* and *F*). Thus, the
266 process of 2C-induced dedifferentiation of CM to RCC is accompanied by vigorous alterations in H3K9Ac,
267 whereas H3K27Ac is remain relatively stable, indicating that the genome-wide distribution of H3K9Ac
268 exhibited drastic distinction between CMs and RCCs. To further confirm this notion, we performed a
269 comparative analysis of annotated genes between the cells treat with 2C or DMSO to validate the most
270 significant differential genes (i.e., Log10LR>3) under the respective condition. In comparison to 430 genes
271 with H3K9Ac enrichment observed in DMSO-treated cells, which were mainly involved in cardiac muscle
272 contraction (Fig. 7 *G* and *H*), 2C treatment markedly enhanced the enrichment of H3K9Ac in 123 genes
273 associated with the transcription factor complex and Wnt signaling pathway (Fig. 7 *I* and *J*). In particular,
274 12 CM genes, including TNNT2, were ranked in top 90 out of 430 annotated genes with H3K9Ac enrichment.
275 In contrast, 7 RCC genes, including ISL1, were ranked in the top 50 out of 123 annotated genes with
276 H3K9Ac enrichment. Moreover, DNA-binding motif analysis indicated that the ISL1 binding motifs only
277 exhibited accessibility in the cells treated with A-485 or 2C (Fig. 7*K*), underscoring the vital role of A-485 in
278 2C treatment to activate the expression of RCC genes. Taken together, these findings revealed that
279 CHIR99021 is responsive for transcriptional and epigenetic activation of genes essential for cardiac
280 embryonic development, while A-485 promotes conversion of CMs to RCCs by epigenetic downregulation
281 of H3K27Ac and particularly H3K9Ac in CMs, which together facilitate the induction of RCCs from CMs.

282 **Discussion**

283 It is worth noting that the RCCs were only generated in hearts of 2C-treated postnatal rats, but not in rats
284 after treatment with only 20 mg/kg CHIR99021 or 10 mg/kg A-485 alone (*SI Appendix,* Fig. S8), indicating
285 the reprogramming of endogenous CMs to RCCs depends on the cooperative effect from these two
286 molecules. CHIR99021 has been well characterized as a GSK3 inhibitor to activate the Wnt signaling
287 pathway. Previous studies have elucidated the role of CHIR99021 in initiating proliferation of hPSC-derived
288 CMs (Buikema *et al*, 2020; Quaife-Ryan *et al*, 2020), accompanied by induction of H3K27Ac on promoter

289 regions of multiple cardiac lineage genes, including TNNT2, MYH6, and ISL1 (Quaife-Ryan *et al.*, 2020).
290 However, this proliferation was only achieved in neonatal CMs *in vivo* (Buikema *et al.*, 2020; Quaife-Ryan
291 *et al.*, 2020). Consistently, we also found the enhanced levels of H3K27Ac in TNNT2$^+$ CMs by treatment
292 with CHIR99021 alone or 2C (Fig. 7*D* and *SI Appendix,* Fig. S10*F*). In addition, we found that the p300/CBP
293 inhibitor A-485 facilitate the reprogramming of CMs into RCCs by epigenetically inhibiting expression of
294 CM-specific genes such as TNNT2 (Fig. 7*D* and *SI Appendix,* Fig. S9*D*), while enhancing the modifications
295 of H3K9Ac and H3K27Ac on RCC-specific genes such as ISL1 in combination with CHIR99021 (Fig. 7 *D*
296 and *K*). These findings promoted us to postulate that A-485 and its mediated mechanism may be used to
297 modulate the cell fate of other terminally differentiated cells by epigenetically suppressing the expression
298 of corresponding lineages specific genes.

299 2C-induced RCCs exhibited potential to differentiate into three cardiac-lineages of the heart *in vitro*,
300 which might contribute additional beneficial effects in heart repair and regeneration. Furthermore, RCCs
301 expressed a broad set of genes essential for embryonic cardiogenesis (Fig. 1*J* and Fig. 5*G*), including ISL1,
302 and a series of potentially important genes identified in this study (Fig. 6*G*), all of which were highly
303 expressed in ISL1$^+$ SHF cardiac progenitors during mammalian heart development. However, RCCs had a
304 restricted proliferation capacity, although they were able to be passaged 3-5 times under 2C conditions
305 (data not shown), which is distinct to ISL1$^+$ cardiac progenitors (Bu *et al.*, 2009; Moretti *et al.*, 2006). These
306 findings collectively indicated that 2C-induced RCCs dedifferentiated from CMs may be expandable under
307 an appropriate condition and deserve further investigation.

308 **References**

309 1. Andersen P, Tampakakis E, Jimenez DV, Kannan S, Miyamoto M, Shin HK, Saberi A, Murphy S,
310 Sulistio E, Chelko SP *et al* (2018) Precardiac organoids form two heart fields via Bmp/Wnt signaling.
311 *Nat Commun* 9: 3140
312 2. Bu L, Jiang X, Martin-Puig S, Caron L, Zhu S, Shao Y, Roberts DJ, Huang PL, Domian IJ, Chien KR
313 (2009) Human ISL1 heart progenitors generate diverse multipotent cardiovascular cell lineages.
314 *Nature* 460: 113-117
315 3. Buikema JW, Lee S, Goodyer WR, Maas RG, Chirikian O, Li G, Miao Y, Paige SL, Lee D, Wu H *et al*
316 (2020) Wnt Activation and Reduced Cell-Cell Contact Synergistically Induce Massive Expansion of
317 Functional Human iPSC-Derived Cardiomyocytes. *Cell Stem Cell* 27: 50-63 e55
318 4. Churko JM, Garg P, Treutlein B, Venkatasubramanian M, Wu H, Lee J, Wessells QN, Chen SY, Chen
319 WY, Chetal K *et al* (2018) Defining human cardiac transcription factor hierarchies using integrated
320 single-cell heterogeneity analysis. *Nat Commun* 9: 4906
321 5. Cohen ED, Wang Z, Lepore JJ, Lu MM, Taketo MM, Epstein DJ, Morrisey EE (2007) Wnt/beta-
322 catenin signaling promotes expansion of Isl-1-positive cardiac progenitor cells through regulation of
323 FGF signaling. *J Clin Invest* 117: 1794-1804
324 6. Cui M, Wang Z, Chen K, Shah AM, Tan W, Duan L, Sanchez-Ortiz E, Li H, Xu L, Liu N *et al* (2020)
325 Dynamic Transcriptional Responses to Injury of Regenerative and Non-regenerative Cardiomyocytes
326 Revealed by Single-Nucleus RNA Sequencing. *Developmental Cell* 53: 102-116.e108
327 7. Ghazizadeh Z, Fattahi F, Mirzaei M, Bayersaikhan D, Lee J, Chae S, Hwang D, Byun K, Tabar MS,
328 Taleahmad S *et al* (2018) Prospective Isolation of ISL1(+) Cardiac Progenitors from Human ESCs for
329 Myocardial Infarction Therapy. *Stem Cell Reports* 10: 848-859
330 8. Kikuchi K, Poss KD (2010) Primary contribution to zebrafish heart regeneration by gata4(+)
331 cardiomyocytes. *Nature* 464: 601-605
332 9. Klaus A, Saga Y, Taketo MM, Tzahor E, Birchmeier W (2007) Distinct roles of Wnt/beta-catenin and
333 Bmp signaling during early cardiogenesis. *Proc Natl Acad Sci U S A* 104: 18531-18536
334 10. Lasko LM, Jakob CG, Edalji RP, Qiu W, Montgomery D, Digiammarino EL, Hansen TM, Risi RM,
335 Frey R, Manaves V *et al* (2017) Discovery of a selective catalytic p300/CBP inhibitor that targets
336 lineage-specific tumours. *Nature* 550: 128-132
337 *11.* Laugwitz K-L (2005) Postnatal isl1 cardioblasts enter fully differentiated cardiomyocyte lineages.
338 *Nature*
339 12. Lepilina A, Coon AN, Kikuchi K, Holdway JE, Roberts RW, Burns CG, Poss KD (2006) A dynamic
340 epicardial injury response supports progenitor cell activity during zebrafish heart regeneration. *Cell*
341 127: 607-619
342 13. Lian X, Zhang J, Azarin SM, Zhu K, Hazeltine LB, Bao X, Hsiao C, Kamp TJ, Palecek SP (2013)
343 Directed cardiomyocyte differentiation from human pluripotent stem cells by modulating Wnt/beta-
344 catenin signaling under fully defined conditions. *Nat Protoc* 8: 162-175
345 14. Liu Y, Bai H, Guo F, Thai PN, Luo X, Zhang P, Yang C, Feng X, Zhu D, Guo J *et al* (2020) PGC-
346 1alpha activator ZLN005 promotes maturation of cardiomyocytes derived from human embryonic
347 stem cells. *Aging (Albany NY)* 12: 7411-7430
348 15. Ma Q, Zhou B, Pu WT (2008) Reassessment of Isl1 and Nkx2-5 cardiac fate maps using a Gata4-
349 based reporter of Cre activity. *Dev Biol* 323: 98-104
350 *16.* Mononen MM, Leung CY, Xu J, Chien KR (2020) Trajectory mapping of human embryonic stem cell
351 cardiogenesis reveals lineage branch points and an ISL1 progenitor-derived cardiac fibroblast
352 lineage. *Stem Cells*
353 17. Moretti A, Caron L, Nakano A, Lam JT, Bernshausen A, Chen Y, Qyang Y, Bu L, Sasaki M, Martin-
354 Puig S *et al* (2006) Multipotent embryonic isl1+ progenitor cells lead to cardiac, smooth muscle, and
355 endothelial cell diversification. *Cell* 127: 1151-1165
356 18. Porrello ER, Mahmoud AI, Simpson E, Hill JA, Richardson JA, Olson EN, Sadek HA (2011) Transient
357 regenerative potential of the neonatal mouse heart. *Science* 331: 1078-1080
358 19. Quaife-Ryan GA, Mills RJ, Lavers G, Voges HK, Vivien CJ, Elliott DA, Ramialison M, Hudson JE,
359 Porrello ER (2020) beta-Catenin drives distinct transcriptional networks in proliferative and
360 nonproliferative cardiomyocytes. *Development* 147
361 20. Sakurai T, Lanahan A, Woolls MJ, Li N, Tirziu D, Murakami M (2014) Live cell imaging of primary rat
362 neonatal cardiomyocytes following adenoviral and lentiviral transduction using confocal spinning disk
363 microscopy. *J Vis Exp*: e51666

21. Srivastava D (2006) Making or breaking the heart: from lineage determination to morphogenesis. *Cell* 126: 1037-1048
22. Wang J, Liu M, Wu Q, Li Q, Gao L, Jiang Y, Deng B, Huang W, Bi W, Chen Z *et al* (2019) Human Embryonic Stem Cell-Derived Cardiovascular Progenitors Repair Infarcted Hearts Through Modulation of Macrophages via Activation of Signal Transducer and Activator of Transcription 6. *Antioxid Redox Signal* 31: 369-386
23. Watanabe Y, Zaffran S, Kuroiwa A, Higuchi H, Ogura T, Harvey RP, Kelly RG, Buckingham M (2012) Fibroblast growth factor 10 gene regulation in the second heart field by Tbx1, Nkx2-5, and Islet1 reveals a genetic switch for down-regulation in the myocardium. *Proc Natl Acad Sci U S A* 109: 18273-18280

Acknowledgments

We thank the Center for Pharmaceutical Technology, Tsinghua University for the activity screening platform, Biomarker Technologies Corporation, Beijing, China and BeiJing Geek Gene Technology Co Ltd for technical support, and support from Tsinghua-Peking Center for Life Sciences.

Author Contributions

Conceptualization, S.D. and W.Z.; Methodology, W.Z., H.L., T.H.M. and Y.N.; Investigation, W.Z., C.Y.W., K.Z.H., P.Q.W., B.W.W., and H.G.; Visualization, W.Z., P.Q.W., B.W.W., H.G., and D.W.; Funding Acquisition, S.D., T.H.M., and Y.N.; Project Administration, W.Z., H.L., T.H.M., and Y.N.; Supervision: S.D., and W.Z.; Writing – Original Draft, W.Z., T.H.M., and S.D.; Writing – Review & Editing: W.Z., T.H.M., Y.N., S.D.

Competing Interests

The authors declare no competing interests.

Data and Materials availability

All targeted amplicon sequencing data have been deposited in the Sequence Read Archive of the NCBI under the BioProject accession number PRJNA903530. All data are available in the main text or the supplementary materials.

Figure and Figure legends

Fig. 1. 2C treatment induced dedifferentiation of hESC-derived CMs toward ISL1-expressing cells. Cells induced from hESC-derived CMs by treatment with DMSO (NC) or 2C for 60 hours. **A,** Phase contrast images showing cell morphology. **B,** Immunofluorescence staining of the ISL1 (ISL1, green), and the CM marker cardiac troponin T (TNNT2, red) in the cells. Nuclei were stained by DAPI (4′,6-diamidino-2-phenylindole) and presented in DNA blue. **(C** and **D)**, Cytosolic (**C**) and nuclear (**D**) areas of the cells. **E**, The number of total cells, TNNT2+ cells, and ISL1$^+$ cells. **F**, Cell percentage of TNNT2$^+$ cells. **G**, Fraction of ISL1$^+$ cell in TNNT2$^+$ cells. Error bars represent SD. ns, not significant (P > 0.05); **P < 0.01; ***P < 0.001. (**H** and **I)** Western blot (**H**) and quantitative analysis (**I**) of ISL1 expression in DMSO (NC) or 2C-treated CMs for 60 hours. Error bars represent SD. *P < 0.05; **J**, Heatmap illustration showing the fold-changes of indicted marker genes' expression by 2C treatment, which were measured using qRT-PCR.

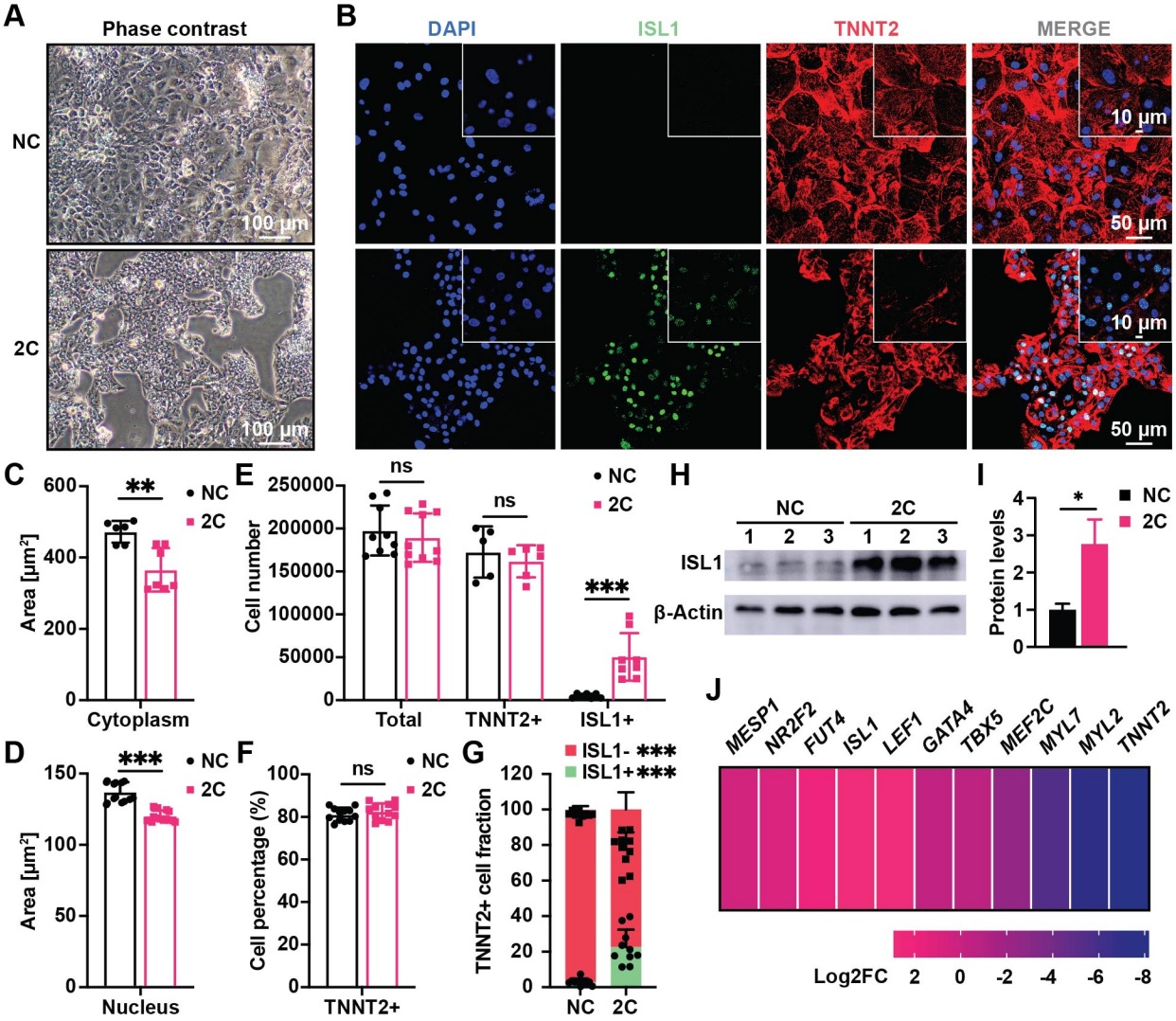

404 **Fig. 2. Regenerative ability of 2C-induced RCCs.** (**A**-**C**)**,** Immunofluorescence staining (**A**) and statistical
405 analysis (**B** and **C**) of the ISL1 (green) and BrdU (red) double positive RCCs induced from CMs by treatment
406 with DMSO (NC) or 2C for 60 hours. DAPI (4′,6-diamidino-2-phenylindole) staining labeled nuclei as blue.
407 Error bars represent SD. **P < 0.01. **D,** Phase contrast images of hESC-derived CMs treated by DMSO
408 (NC) or 2C for 60 hours (60h) and subsequently cultured in the absence of 2C for another 3 days (60h+3d).
409 (**E** and **F**)**,** Cytosolic (**E**) and nuclear (**F**) areas of the cells under the same condition in (**D**). Error bars
410 indicate SD. ns, not significant (P > 0.05); ***P < 0.001. **G,** Immunostaining showed the expression of ISL1
411 (green) and TNNT2 (red) in the cells under the same condition in (**D**). **H,** The fold change of $TNNT2^{+}$ cells
412 under the same condition in (**D**). Error bars represent SD. ns, not significant (P > 0.05); **P < 0.01.
413 Immunostaining showed the expression of EC markers (CD31, green and CD144, red), SMC marker (SMA,
414 red), and CM marker (TNNT2, green).

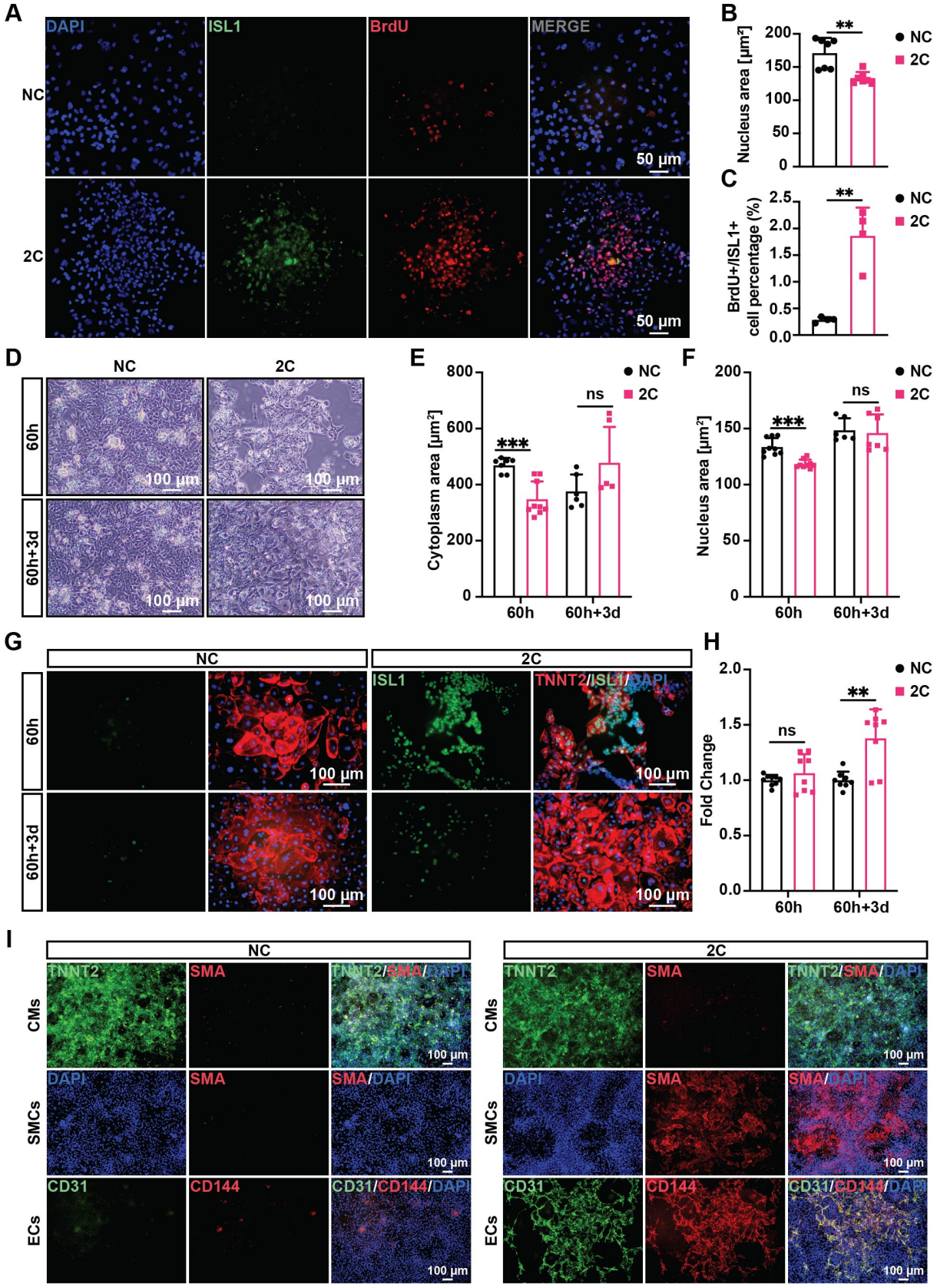
A
DAPI
ISL1
BrdU
MERGE
NC
2C
50 μm
B
Nucleus area [μm²]
**
NC
2C
C
BrdU+/ISL1+ cell percentage (%)
**
D
NC
2C
60h
60h+3d
100 μm
E
Cytoplasm area [μm²]
***
ns
F
Nucleus area [μm²]
***
ns
G
ISL1
TNNT2/ISL1/DAPI
H
Fold Change
ns
**
I
TNNT2
SMA
TNNT2/SMA/DAPI
CMs
DAPI
SMA/DAPI
SMCs
CD31
CD144
CD31/CD144/DAPI
ECs

415

Fig. 3. Lineage tracing demonstrated 2C induced dedifferentiation of TNNT2+ CMs to ISL1-expressing RCCs. A, Immunofluorescence images showing expression of endogenous ISL1 (green) and ISL1-mCherry (red) reporter in the cells differentiated from K9 hESC KI reporter line at day 6 (D6). (**B** and **C**) Flow cytometry analysis of the percentage of mCherry^{+}/ISL1^{+} cells in the cells differentiated from K9 at D6. (**D** and **E**) Flow cytometry analysis of the percentage of mCherry-negative cells at selection day 4 (SD4) in lactate purification medium. Error bars represent SD. (**F**-**H**) Cells induced from mCherry-negative CMs by treatment with or without 2C for 60 hours. Images showing the expression of mCHERRY (red) and TNNT2 (green) in the cells (**F**) and flow cytometry analysis of the percentage of mCherry-positive cells (**G** and **H**). Error bars represent SD. (**I** and **J**) Flow cytometry analysis of the percentage of mCherry-positive cells dedifferentiated from K7 hESC KI reporter line derived mCherry-negative CMs. Error bars represent SD. **(K** and **L),** Relative gene expression of ISL1, mCHERRY, LEF1, TNNT2 and MYL2 in K9- and K7-derived mCherry-negative CMs treated with DMSO (NC) or 2C for 60 hours, respectively. Error bars represent SD. *P < 0.05; **P < 0.01; ***P < 0.001. (**M** and **N)** Flow cytometric plots showing EGFP-labeled CMs by lineage-tracing of K9-derived mCherry-negative CMs (**M**), and bar graph showing the percentage of mCherry-negative CMs expressing EGFP (**N**). Error bars represent SD. **O,** Images showing the expression of ISL1 (red) and EGFP (green) in the cells induced from EGFP-positive/mCherry-negative CMs in (**M**) by treatment with or without 2C for 60 hours.

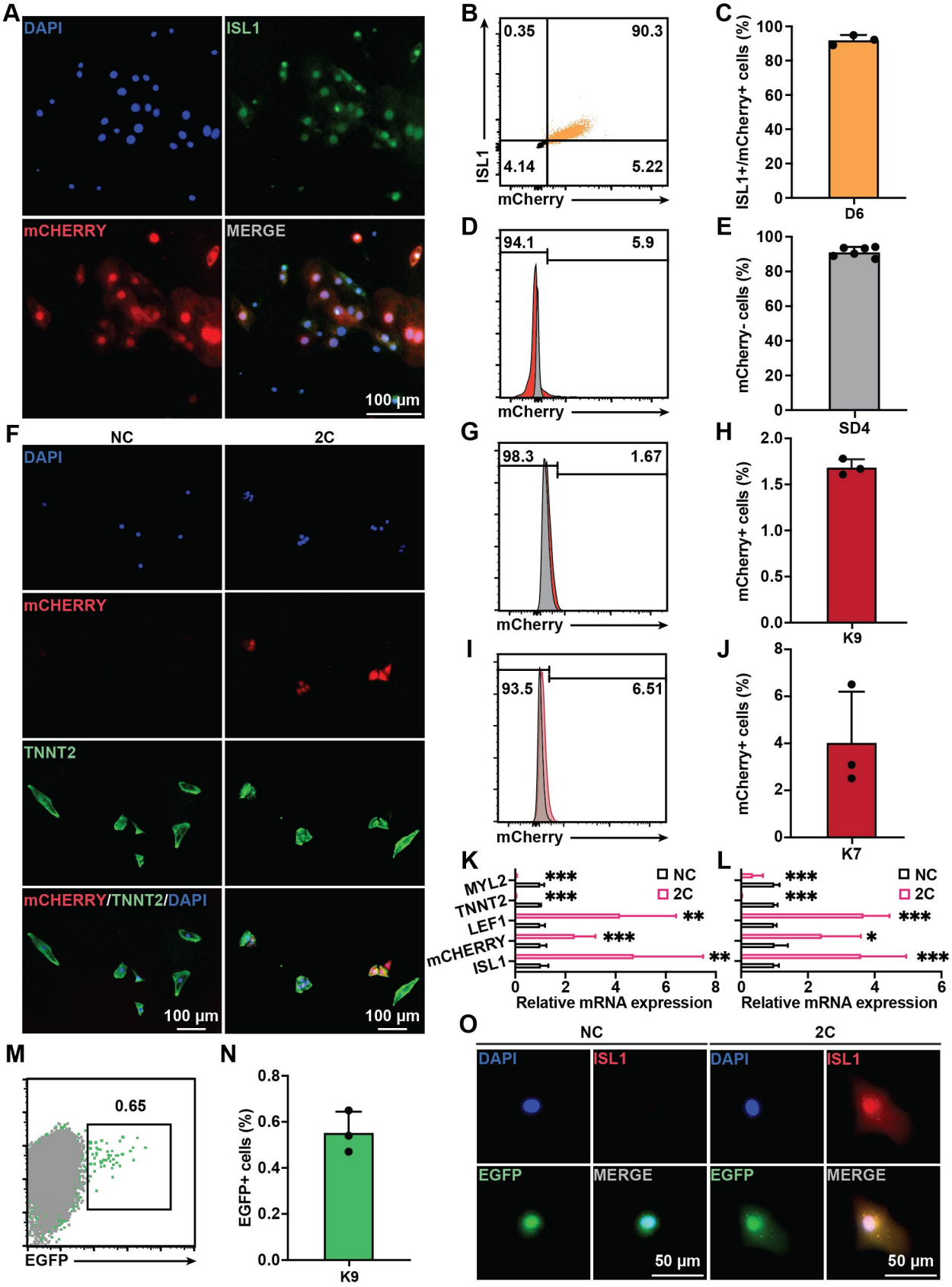
A
DAPI
ISL1
mCHERRY
MERGE
100 μm
B
0.35
90.3
4.14
5.22
ISL1
mCherry
C
ISL1+/mCherry+ cells (%)
D6
D
94.1
5.9
mCherry
E
mCherry- cells (%)
SD4
F
NC
2C
DAPI
mCHERRY
TNNT2
mCHERRY/TNNT2/DAPI
100 μm
G
98.3
1.67
mCherry
H
mCherry+ cells (%)
K9
I
93.5
6.51
mCherry
J
mCherry+ cells (%)
K7
K
MYL2
TNNT2
LEF1
mCHERRY
ISL1
NC
2C
Relative mRNA expression
L
Relative mRNA expression
M
0.65
EGFP
N
EGFP+ cells (%)
K9
O
NC
2C
DAPI
ISL1
EGFP
MERGE
50 μm

436 **Fig. 4. Heart regeneration *via* 2C-induced dedifferentiation of CMs. A,** Immunofluorescence staining of
437 ISL1 (green) and TNNT2 (red) in cross-sectioned hearts from 2C or vehicle-treated (NC) adult 129SvJ mice.
438 Ao, aorta. PA, pulmonary artery. LA, left atrial. RA, right atrial. IAS, interatrial septum. **B,** Schematic
439 illustration of the method used to examine the prophylactic effect of 2C in 129SvJ mice post MI. **C,** Body
440 weight of mice pre-treated with vehicle (DMSO) or 2C as shown in (**B**) at Day 12, Day 16, Day20, and
441 Day35 after MI (1dpi). Error bars represent SD. ns, not significant ($P > 0.05$). **D,** Survival curve of sham-
442 operated mice and mice pre-treated with vehicle (DMSO) or 2C as shown in (**B**), at indicated time points
443 before or after MI. **E,** Ejection fraction (EF) of sham-operated mice and mice pre-treated with vehicle (DMSO)
444 or 2C as shown in (**B**), before MI (baseline) or at Day 1, Day8, Day25, and Day35 after MI (1dpi). Error bars
445 represent SD. ns, not significant ($P > 0.05$); $^{**}P < 0.01$; $^{***}P < 0.001$. **F,** Schematic illustration of the method
446 used to examine therapeutic effect of 2C in the 129SvJ mice post MI. **G,** Echocardiography of sham-
447 operated mice and mice treated with vehicle (DMSO) or 2C as shown in (**F**) at Day 35 post MI. **H,** Serial
448 fMRI measurements showing the cardiac function from sham-operated mice and mice treated with vehicle
449 (DMSO) or 2C at as shown in (**F**), at Day 35 post MI. Error bars represent SD. $^{*}P < 0.05$. **I,** Masson staining
450 of serial transverse sections of hearts from sham-operated mice and mice treated with vehicle (DMSO) or
451 2C as shown in (**F**), at Day 35 post MI.

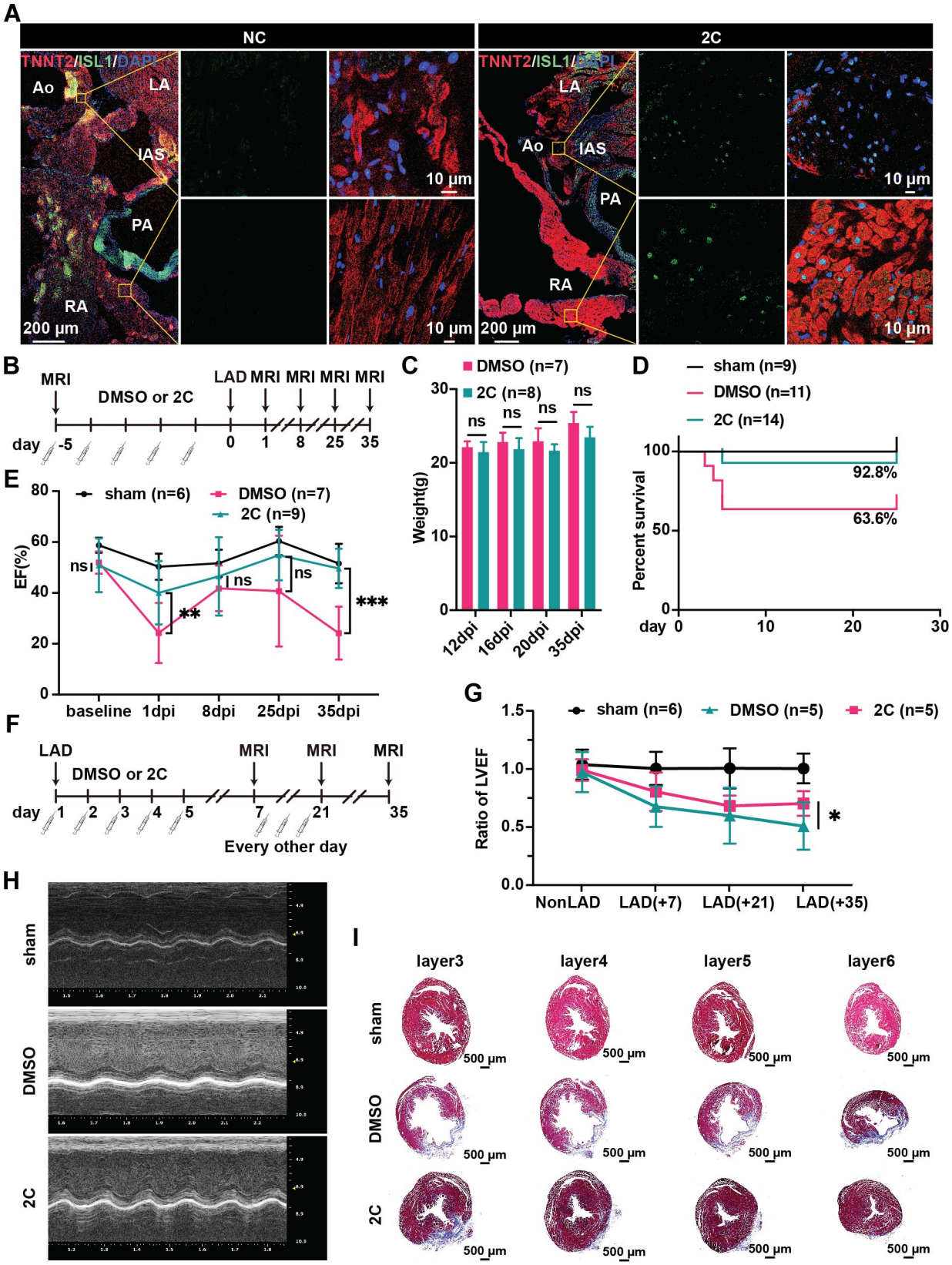
A
NC
2C
TNNT2/ISL1/DAPI
Ao
LA
IAS
PA
RA
200 μm
10 μm
B
MRI
DMSO or 2C
LAD MRI MRI MRI MRI
day -5 0 1 8 25 35
C
DMSO (n=7)
2C (n=8)
Weight(g)
ns
12dpi
16dpi
20dpi
35dpi
D
sham (n=9)
DMSO (n=11)
2C (n=14)
Percent survival
92.8%
63.6%
day
E
sham (n=6)
DMSO (n=7)
2C (n=9)
EF(%)
ns
**
***
baseline
1dpi
8dpi
25dpi
35dpi
F
LAD
DMSO or 2C
MRI
day 1 2 3 4 5 7 21 35
Every other day
G
sham (n=6)
DMSO (n=5)
2C (n=5)
Ratio of LVEF
*
NonLAD
LAD(+7)
LAD(+21)
LAD(+35)
H
sham
DMSO
2C
I
layer3
layer4
layer5
layer6
500 μm

452

453 **Fig. 5. Bulk RNA-seq of analysis of 2C-treated ISL1/mCherry-negative CMs. A,** Scheme of bulk RNA-
454 seq analysis of K9-derived mCherry-negative CMs with DMSO (NC) or 2C treatment for 60 hours. **B,**
455 Heatmap of differentially expressed genes (DEGs) in ISL1/mCherry-negative CMs treated with DMSO (NC)
456 or 2C for 60 hours. **C**, Volcano plot showing genes significantly changed by 60 hours of 2C treatment. (**D**
457 and **E**) Gene Ontology (GO) analysis of downregulated (**D**) and upregulated (**E**) genes in ISL1/mCherry-
458 negative CMs by 2C treatment for 60 hours, compared to DMSO (NC) treated cells. **F,** Plotting GO terms
459 of upregulated genes by 2C treatment with cnetlpot. **G,** Relative expression fold-changes of indicated genes
460 in K9-derived ISL1/mCherry-negative CMs by 60 hours of DMSO (NC) or 2C treatment. Error bars indicate
461 SD. **P < 0.01; ***P < 0.001.

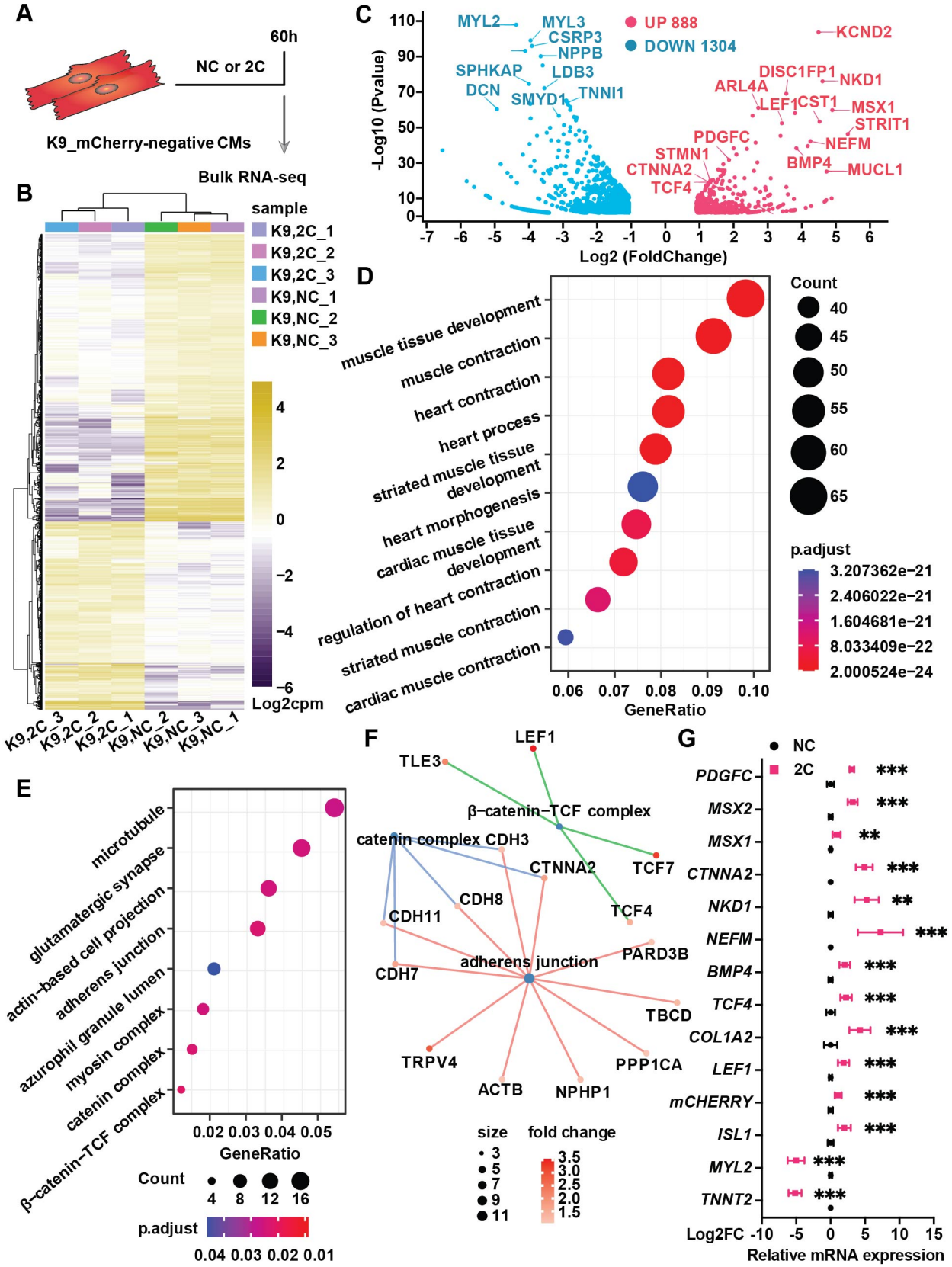
A
60h
NC or 2C
K9_mCherry-negative CMs
Bulk RNA-seq
B
sample
K9,2C_1
K9,2C_2
K9,2C_3
K9,NC_1
K9,NC_2
K9,NC_3
Log2cpm
C
UP 888
DOWN 1304
-Log10 (Pvalue)
Log2 (FoldChange)
MYL2
MYL3
CSRP3
NPPB
SPHKAP
LDB3
DCN
SMYD1
TNNI1
KCND2
DISC1FP1
NKD1
ARL4A
LEF1
CST1
MSX1
STRIT1
PDGFC
NEFM
STMN1
BMP4
CTNNA2
MUCL1
TCF4
D
muscle tissue development
muscle contraction
heart contraction
heart process
striated muscle tissue development
heart morphogenesis
cardiac muscle tissue development
regulation of heart contraction
striated muscle contraction
cardiac muscle contraction
GeneRatio
Count
p.adjust
3.207362e−21
2.406022e−21
1.604681e−21
8.033409e−22
2.000524e−24
E
microtubule
glutamatergic synapse
actin-based cell projection
adherens junction
azurophil granule lumen
myosin complex
catenin complex
β-catenin-TCF complex
GeneRatio
Count
p.adjust
F
LEF1
TLE3
β-catenin-TCF complex
catenin complex CDH3
CTNNA2
TCF7
CDH8
TCF4
CDH11
adherens junction
PARD3B
CDH7
TBCD
TRPV4
PPP1CA
ACTB
NPHP1
size
fold change
G
NC
2C
PDGFC
MSX2
MSX1
CTNNA2
NKD1
NEFM
BMP4
TCF4
COL1A2
LEF1
mCHERRY
ISL1
MYL2
TNNT2
Log2FC
Relative mRNA expression

462

463 **Fig. 6. Single-cell RNA-seq of 2C-treated mCherry-negative CMs. A,** UMAP analysis showing 7 clusters
464 in cells induced from K9-derived mCherry-negative CMs by treatment with DMSO (NC) and 2C for 60 hours.
465 **B,** The percentage of cells in the 7 indicated clusters, following DMSO (NC) or 2C treatment. **C,** Heatmap
466 showing the differentially expressed genes in the cells from 7 indicated clusters. The representative marker
467 genes of 7 indicated clusters were listed on the right. **D,** Violin plots showing the expression levels of marker
468 genes of CMs (MYL2, MYH6), ICs (COL1A1, ACTA2), and RCCs (ISL1, BMP4, FGF20) among cells from
469 7 indicated clusters. **E,** UMAP analysis showing the second-level clustering of cluster 2 into 4 subclusters
470 (left), which exhibited dramatic distinction under condition of 2C or NC (right). **F,** The percentage of cells in
471 the 4 indicated subclusters within cluster 2, following DMSO (NC) or 2C treatment. **G,** Heatmap showing
472 the differentially expressed genes among cells from 4 subclusters of cluster 2. Genes related to RCCs are
473 highlighted in the green blocks on the right. (**H** and **I**) Pseudotime trajectory showing changes across
474 various cell states upon 2C treatment, which were presented with different developmental pseudotime
475 points (**H**) and cell states (**I**). **J,** Curves showing the dynamic expression of representative genes of RCCs
476 (ISL1, FGF20), ICs (COL1A1), and CMs (TNNT2) along indicated pseudotime points.
477

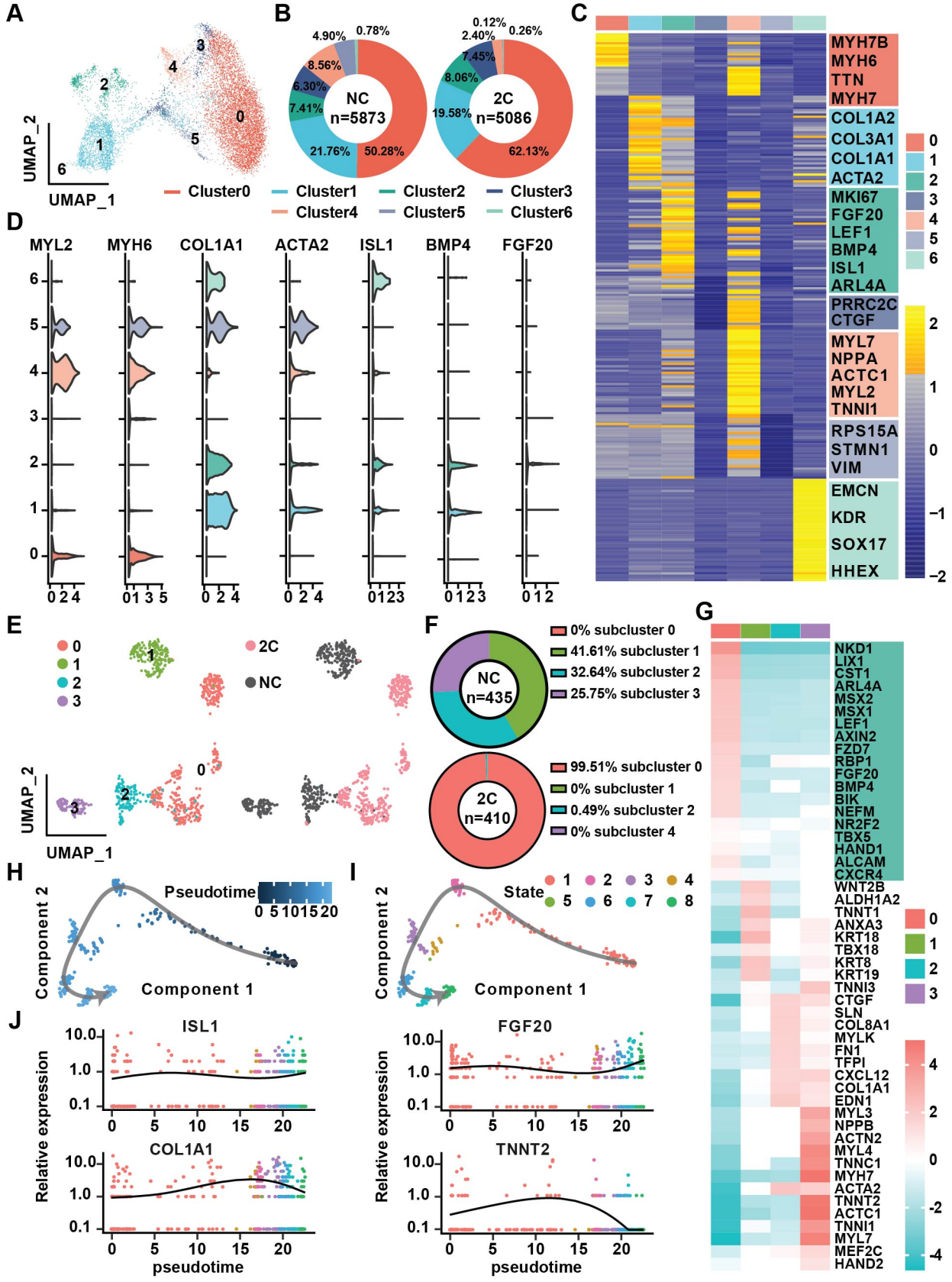
A
UMAP_2
UMAP_1
Cluster0
Cluster1
Cluster2
Cluster3
Cluster4
Cluster5
Cluster6
B
NC
n=5873
2C
n=5086
C
MYH7B
MYH6
TTN
MYH7
COL1A2
COL3A1
COL1A1
ACTA2
MKI67
FGF20
LEF1
BMP4
ISL1
ARL4A
PRRC2C
CTGF
MYL7
NPPA
ACTC1
MYL2
TNNI1
RPS15A
STMN1
VIM
EMCN
KDR
SOX17
HHEX
D
MYL2
MYH6
COL1A1
ACTA2
ISL1
BMP4
FGF20
E
2C
NC
F
NC
n=435
0% subcluster 0
41.61% subcluster 1
32.64% subcluster 2
25.75% subcluster 3
2C
n=410
99.51% subcluster 0
0% subcluster 1
0.49% subcluster 2
0% subcluster 4
G
NKD1
LIX1
CST1
ARL4A
MSX2
MSX1
LEF1
AXIN2
FZD7
RBP1
FGF20
BMP4
BIK
NEFM
NR2F2
TBX5
HAND1
ALCAM
CXCR4
WNT2B
ALDH1A2
TNNT1
ANXA3
KRT18
TBX18
KRT8
KRT19
TNNI3
CTGF
SLN
COL8A1
MYLK
FN1
TFPI
CXCL12
COL1A1
EDN1
MYL3
NPPB
ACTN2
MYL4
TNNC1
MYH7
ACTA2
TNNT2
ACTC1
TNNI1
MYL7
MEF2C
HAND2
H
Pseudotime
Component 2
Component 1
I
State
J
ISL1
COL1A1
FGF20
TNNT2
Relative expression
pseudotime

478

Fig. 7. Chromatin immunoprecipitation-sequencing (ChIP-seq) analyses of chemical-treated H9 hESC-derived CMs. A, Schematic illustration of ChIP-seq analysis of H9-derived CMs subjected to DMSO, A-485, CHIR99021, or 2C treatment for 60 hours. **B,** Average ChIP-seq signal profiles showing the indicated histone modifications around the TSS in the input and ChIP samples prepared from DMSO and 2C-treated cells. **C,** Heatmap showing the whole-genome wide distribution of H3K9Ac, H3K27Ac, and H3K4me3 peaks within a range of ±4kb from TSSs in the cells treated with DMSO or 2C for 60 hours. **D,** H3K9Ac and H3K27Ac peaks surrounding CM genes (TNNT2 and TNNI1) and RCC genes (LEF1 and ISL1) in the cells treated with DMSO, A-485, CHIR99021 or 2C for 60 hours, and H3K4me3 peaks surrounding the same genes in the cells treated by DMSO or 2C. **E,** Veen diagram showing the number of annotated genes with H3K9Ac or H3K27Ac enrichment in the cells treated with DMSO, A-485, CHIR99021 or 2C for 60 hours. Red circles indicate the number of genes with unique H3K9Ac or H3K27Ac enrichment induced by 2C treatment; black circles indicate the number of genes with H3K9Ac or H3K27Ac enrichment unaffected by any chemical treatment. (**G**-**J**) The annotated genes with the most significant changes in H3K9Ac enrichment following treatment with DMSO (**G**) or 2C (**I**) were ranked by Log10LR and analyzed by GOs (**H** and **J**), respectively. **K,** ISL1 binding motifs identified from the cells treated with A-485 or 2C.

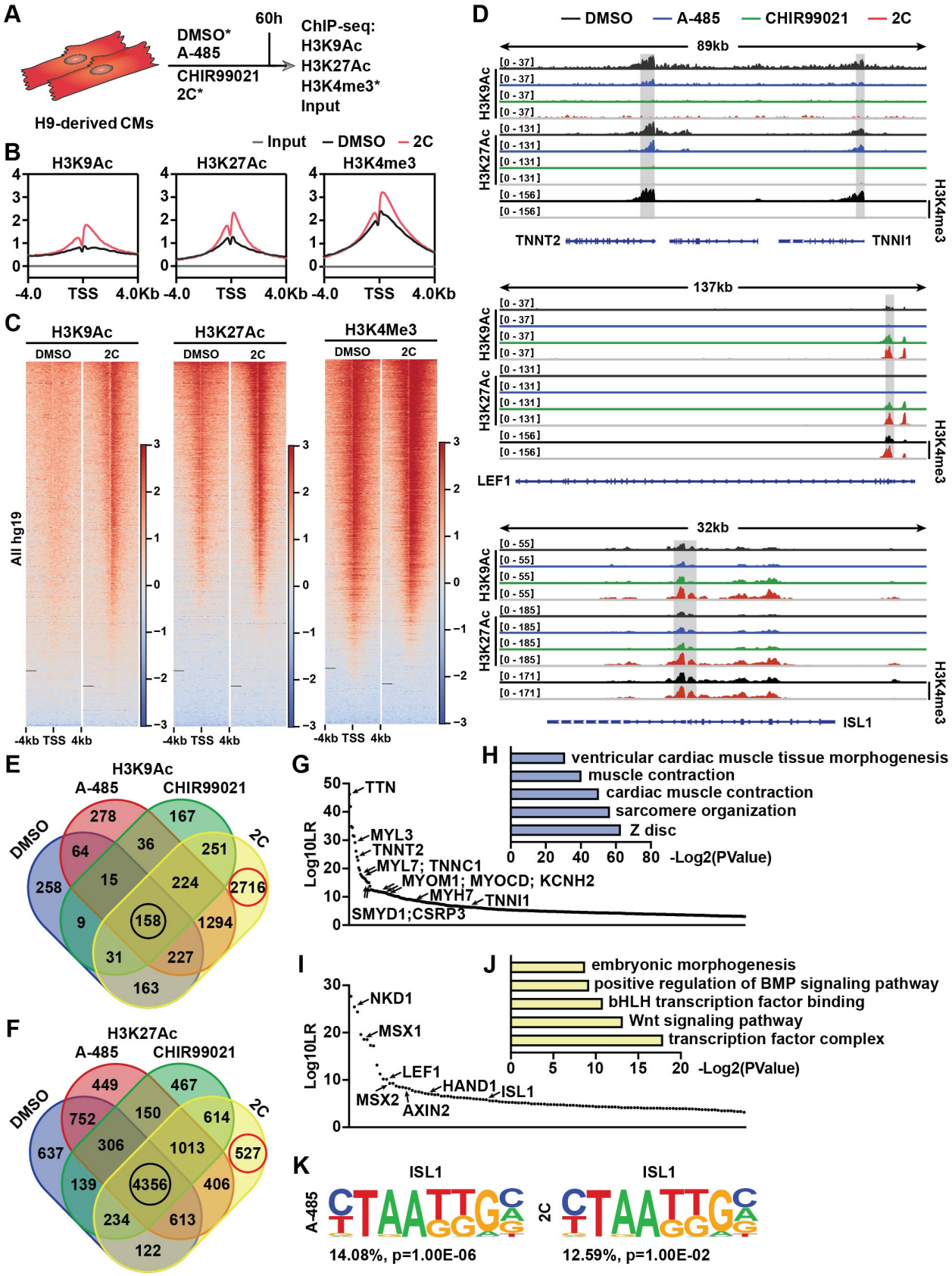
A
H9-derived CMs
DMSO*
A-485
CHIR99021
2C*
60h
ChIP-seq:
H3K9Ac
H3K27Ac
H3K4me3*
Input
B
Input
DMSO
2C
H3K9Ac
H3K27Ac
H3K4me3
-4.0
TSS
4.0Kb
C
H3K9Ac
H3K27Ac
H3K4Me3
DMSO
2C
All hg19
-4kb TSS 4kb
D
DMSO
A-485
CHIR99021
2C
89kb
H3K9Ac
H3K27Ac
H3K4me3
TNNT2
TNNI1
137kb
LEF1
32kb
ISL1
E
H3K9Ac
A-485
CHIR99021
DMSO
2C
278
167
64
36
251
258
15
224
2716
9
158
1294
31
227
163
F
H3K27Ac
A-485
CHIR99021
DMSO
2C
449
467
752
150
614
637
306
1013
527
139
4356
406
234
613
122
G
Log10LR
TTN
MYL3
TNNT2
MYL7; TNNC1
MYOM1; MYOCD; KCNH2
MYH7
TNNI1
SMYD1;CSRP3
H
ventricular cardiac muscle tissue morphogenesis
muscle contraction
cardiac muscle contraction
sarcomere organization
Z disc
-Log2(PValue)
I
Log10LR
NKD1
MSX1
LEF1
HAND1
ISL1
MSX2
AXIN2
J
embryonic morphogenesis
positive regulation of BMP signaling pathway
bHLH transcription factor binding
Wnt signaling pathway
transcription factor complex
-Log2(PValue)
K
ISL1
A-485
14.08%, p=1.00E-06
ISL1
2C
12.59%, p=1.00E-02